

Limits on gravitational wave emission from selected pulsars using LIGO data

B. Abbott,¹² R. Abbott,¹⁵ R. Adhikari,¹³ A. Ageev,^{20,27} B. Allen,³⁹ R. Amin,³⁴ S. B. Anderson,¹² W. G. Anderson,²⁹ M. Araya,¹² H. Armandula,¹² M. Ashley,²⁸ F. Asiri,^{12, a} P. Aufmuth,³¹ C. Aubert,¹ S. Babak,⁷ R. Balasubramanian,⁷ S. Ballmer,¹³ B. C. Barish,¹² C. Barker,¹⁴ D. Barker,¹⁴ M. Barnes,^{12, b} B. Barr,³⁵ M. A. Barton,¹² K. Bayer,¹³ R. Beausoleil,^{26, c} K. Belczynski,²³ R. Bennett,^{35, d} S. J. Berukoff,^{1, e} J. Betzwieser,¹³ B. Bhawal,¹² I. A. Bilenko,²⁰ G. Billingsley,¹² E. Black,¹² K. Blackburn,¹² L. Blackburn,¹³ B. Bland,¹⁴ B. Bochner,^{13, f} L. Bogue,¹² R. Bork,¹² S. Bose,⁴⁰ P. R. Brady,³⁹ V. B. Braginsky,²⁰ J. E. Brau,³⁷ D. A. Brown,³⁹ A. Bullington,²⁶ A. Bunkowski,^{2,31} A. Buonanno,^{6, g} R. Burgess,¹³ D. Busby,¹² W. E. Butler,³⁸ R. L. Byer,²⁶ L. Cadonati,¹³ G. Cagnoli,³⁵ J. B. Camp,²¹ C. A. Cantley,³⁵ L. Cardenas,¹² K. Carter,¹⁵ M. M. Casey,³⁵ J. Castiglione,³⁴ A. Chandler,¹² J. Chapsky,^{12, b} P. Charlton,¹² S. Chatterji,¹³ S. Chelkowski,^{2,31} Y. Chen,⁶ V. Chikarmane,^{16, h} D. Chin,³⁶ N. Christensen,⁸ D. Churches,⁷ T. Cokelaer,⁷ C. Colacino,³³ R. Coldwell,³⁴ M. Coles,^{15, i} D. Cook,¹⁴ T. Corbitt,¹³ D. Coyne,¹² J. D. E. Creighton,³⁹ T. D. Creighton,¹² D. R. M. Crooks,³⁵ P. Csatorday,¹³ B. J. Cusack,³ C. Cutler,¹ E. D'Ambrosio,¹² K. Danzmann,^{31,2} E. Daw,^{16, j} D. DeBra,²⁶ T. Delker,^{34, k} V. Dergachev,³⁶ R. DeSalvo,¹² S. Dhurandhar,¹¹ A. Di Credico,²⁷ M. Díaz,²⁹ H. Ding,¹² R. W. P. Drever,⁴ R. J. Dupuis,³⁵ J. A. Edlund,^{12, b} P. Ehrens,¹² E. J. Elliffe,³⁵ T. Etzel,¹² M. Evans,¹² T. Evans,¹⁵ S. Fairhurst,³⁹ C. Fallnich,³¹ D. Farnham,¹² M. M. Fejer,²⁶ T. Findley,²⁵ M. Fine,¹² L. S. Finn,²⁸ K. Y. Franzen,³⁴ A. Freise,^{2,1} R. Frey,³⁷ P. Fritschel,¹³ V. V. Frolov,¹⁵ M. Fyffe,¹⁵ K. S. Ganezer,⁵ J. Garofoli,¹⁴ J. A. Giaime,¹⁶ A. Gillespie,^{12, m} K. Goda,¹³ G. González,¹⁶ S. Goßler,³¹ P. Grandclément,^{23, n} A. Grant,³⁵ C. Gray,¹⁴ A. M. Gretarsson,¹⁵ D. Grimmer,¹² H. Grote,² S. Grunewald,¹ M. Guenther,¹⁴ E. Gustafson,^{26, o} R. Gustafson,³⁶ W. O. Hamilton,¹⁶ M. Hammond,¹⁵ J. Hanson,¹⁵ C. Hardham,²⁶ J. Harms,¹⁹ G. Harry,¹³ A. Hartunian,¹² J. Heefner,¹² Y. Hefetz,¹³ G. Heinzl,² I. S. Heng,³¹ M. Hennessy,²⁶ N. Hepler,²⁸ A. Heptonstall,³⁵ M. Heurs,³¹ M. Hewitson,² S. Hild,² N. Hindman,¹⁴ P. Hoang,¹² J. Hough,³⁵ M. Hrynevych,^{12, p} W. Hua,²⁶ M. Ito,³⁷ Y. Itoh,¹ A. Ivanov,¹² O. Jennrich,^{35, q} B. Johnson,¹⁴ W. W. Johnson,¹⁶ W. R. Johnston,²⁹ D. I. Jones,²⁸ L. Jones,¹² D. Jungwirth,^{12, r} V. Kalogera,²³ E. Katsavounidis,¹³ K. Kawabe,¹⁴ S. Kawamura,²² W. Kells,¹² J. Kern,^{15, s} A. Khan,¹⁵ S. Killbourn,³⁵ C. J. Killow,³⁵ C. Kim,²³ C. King,¹² P. King,¹² S. Klimenko,³⁴ S. Koranda,³⁹ K. Kötter,³¹ J. Kovalik,^{15, b} D. Kozak,¹² B. Krishnan,¹ M. Landry,¹⁴ J. Langdale,¹⁵ B. Lantz,²⁶ R. Lawrence,¹³ A. Lazzarini,¹² M. Lei,¹² I. Leonor,³⁷ K. Libbrecht,¹² A. Libson,⁸ P. Lindquist,¹² S. Liu,¹² J. Logan,^{12, t} M. Lormand,¹⁵ M. Lubinski,¹⁴ H. Lück,^{31,2} T. T. Lyons,^{12, t} B. Machenschalk,¹ M. MacInnis,¹³ M. Mageswaran,¹² K. Mailand,¹² W. Majid,^{12, b} M. Malec,^{2,31} F. Mann,¹² A. Marin,^{13, u} S. Márka,¹² E. Maros,¹² J. Mason,^{12, v} K. Mason,¹³ O. Matherny,¹⁴ L. Matone,¹⁴ N. Mavalvala,¹³ R. McCarthy,¹⁴ D. E. McClelland,³ M. McHugh,¹⁸ J. W. C. McNabb,²⁸ G. Mendell,¹⁴ R. A. Mercer,³³ S. Meshkov,¹² E. Messaritaki,³⁹ C. Messenger,³³ V. P. Mitrofanov,²⁰ G. Mitselmakher,³⁴ R. Mittleman,¹³ O. Miyakawa,¹² S. Miyoki,^{12, w} S. Mohanty,²⁹ G. Moreno,¹⁴ K. Mossavi,² G. Mueller,³⁴ S. Mukherjee,²⁹ P. Murray,³⁵ J. Myers,¹⁴ S. Nagano,² T. Nash,¹² R. Nayak,¹¹ G. Newton,³⁵ F. Nocera,¹² J. S. Noel,⁴⁰ P. Nutzman,²³ T. Olson,²⁴ B. O'Reilly,¹⁵ D. J. Ottaway,¹³ A. Ottewill,^{39, x} D. Ouimette,^{12, r} H. Overmier,¹⁵ B. J. Owen,²⁸ Y. Pan,⁶ M. A. Papa,¹ V. Parameshwaraiah,¹⁴ C. Parameswariah,¹⁵ M. Pedraza,¹² S. Penn,¹⁰ M. Pitkin,³⁵ M. Plissi,³⁵ R. Prix,¹ V. Quetschke,³⁴ F. Raab,¹⁴ H. Radkins,¹⁴ R. Rakhola,³⁷ M. Rakhmanov,³⁴ S. R. Rao,¹² K. Rawlins,¹³ S. Ray-Majumder,³⁹ V. Re,³³ D. Redding,^{12, b} M. W. Regehr,^{12, b} T. Regimbau,⁷ S. Reid,³⁵ K. T. Reilly,¹² K. Reithmaier,¹² D. H. Reitze,³⁴ S. Richman,^{13, y} R. Riesen,¹⁵ K. Riles,³⁶ B. Rivera,¹⁴ A. Rizzi,^{15, z} D. I. Robertson,³⁵ N. A. Robertson,^{26,35} L. Robison,¹² S. Roddy,¹⁵ J. Rollins,¹³ J. D. Romano,⁷ J. Romie,¹² H. Rong,^{34, m} D. Rose,¹² E. Rotthoff,²⁸ S. Rowan,³⁵ A. Rüdiger,² P. Russell,¹² K. Ryan,¹⁴ I. Salzman,¹² V. Sandberg,¹⁴ G. H. Sanders,^{12, aa} V. Sannibale,¹² B. Sathyaprakash,⁷ P. R. Saulson,²⁷ R. Savage,¹⁴ A. Sazonov,³⁴ R. Schilling,² K. Schlaufman,²⁸ V. Schmidt,^{12, bb} R. Schnabel,¹⁹ R. Schofield,³⁷ B. F. Schutz,^{1,7} P. Schwinberg,¹⁴ S. M. Scott,³ S. E. Seader,⁴⁰ A. C. Searle,³ B. Sears,¹² S. Seel,¹² F. Seifert,¹⁹ A. S. Sengupta,¹¹ C. A. Shapiro,^{28, cc} P. Shawhan,¹² D. H. Shoemaker,¹³ Q. Z. Shu,^{34, dd} A. Sibley,¹⁵ X. Siemens,³⁹ L. Sievers,^{12, b} D. Sigg,¹⁴ A. M. Sintes,^{1,32} J. R. Smith,² M. Smith,¹³ M. R. Smith,¹² P. H. Sneddon,³⁵ R. Spero,^{12, b} G. Stapfer,¹⁵ D. Steussy,⁸ K. A. Strain,³⁵ D. Strom,³⁷ A. Stuver,²⁸ T. Summerscales,²⁸ M. C. Sumner,¹² P. J. Sutton,¹² J. Sylvestre,^{12, ee} A. Takamori,¹² D. B. Tanner,³⁴ H. Tariq,¹² I. Taylor,⁷ R. Taylor,¹² R. Taylor,³⁵ K. A. Thorne,²⁸ K. S. Thorne,⁶ M. Tibbits,²⁸ S. Tilav,^{12, ff} M. Tinto,^{4, b} K. V. Tokmakov,²⁰ C. Torres,²⁹ C. Torrie,¹² G. Traylor,¹⁵ W. Tyler,¹² D. Ugolini,³⁰ C. Ungarelli,³³ M. Vallisneri,^{6, gg} M. van Putten,¹³ S. Vass,¹² A. Vecchio,³³ J. Veitch,³⁵ C. Vorvick,¹⁴ S. P. Vyachanin,²⁰ L. Wallace,¹² H. Walther,¹⁹ H. Ward,³⁵ B. Ware,^{12, b} K. Watts,¹⁵ D. Webber,¹² A. Weidner,¹⁹ U. Weiland,³¹ A. Weinstein,¹² R. Weiss,¹³ H. Welling,³¹ L. Wen,¹² S. Wen,¹⁶ J. T. Whelan,¹⁸ S. E. Whitcomb,¹² B. F. Whiting,³⁴ S. Wiley,⁵ C. Wilkinson,¹⁴ P. A. Willems,¹² P. R. Williams,^{1, hh} R. Williams,⁴ B. Willke,³¹ A. Wilson,¹² B. J. Winjum,^{28, e} W. Winkler,² S. Wise,³⁴ A. G. Wiseman,³⁹ G. Woan,³⁵ R. Wooley,¹⁵ J. Worden,¹⁴ W. Wu,³⁴ I. Yakushin,¹⁵ H. Yamamoto,¹² S. Yoshida,²⁵

M. Kramer⁴¹ and A. G. Lyne⁴¹

- ¹Albert-Einstein-Institut, Max-Planck-Institut für Gravitationsphysik, D-14476 Golm, Germany
²Albert-Einstein-Institut, Max-Planck-Institut für Gravitationsphysik, D-30167 Hannover, Germany
³Australian National University, Canberra, 0200, Australia
⁴California Institute of Technology, Pasadena, CA 91125, USA
⁵California State University Dominguez Hills, Carson, CA 90747, USA
⁶Caltech-CaRT, Pasadena, CA 91125, USA
⁷Cardiff University, Cardiff, CF2 3YB, United Kingdom
⁸Carleton College, Northfield, MN 55057, USA
⁹Fermi National Accelerator Laboratory, Batavia, IL 60510, USA
¹⁰Hobart and William Smith Colleges, Geneva, NY 14456, USA
¹¹Inter-University Centre for Astronomy and Astrophysics, Pune - 411007, India
¹²LIGO - California Institute of Technology, Pasadena, CA 91125, USA
¹³LIGO - Massachusetts Institute of Technology, Cambridge, MA 02139, USA
¹⁴LIGO Hanford Observatory, Richland, WA 99352, USA
¹⁵LIGO Livingston Observatory, Livingston, LA 70754, USA
¹⁶Louisiana State University, Baton Rouge, LA 70803, USA
¹⁷Louisiana Tech University, Ruston, LA 71272, USA
¹⁸Loyola University, New Orleans, LA 70118, USA
¹⁹Max Planck Institut für Quantenoptik, D-85748, Garching, Germany
²⁰Moscow State University, Moscow, 119992, Russia
²¹NASA/Goddard Space Flight Center, Greenbelt, MD 20771, USA
²²National Astronomical Observatory of Japan, Tokyo 181-8588, Japan
²³Northwestern University, Evanston, IL 60208, USA
²⁴Salish Kootenai College, Pablo, MT 59855, USA
²⁵Southeastern Louisiana University, Hammond, LA 70402, USA
²⁶Stanford University, Stanford, CA 94305, USA
²⁷Syracuse University, Syracuse, NY 13244, USA
²⁸The Pennsylvania State University, University Park, PA 16802, USA
²⁹The University of Texas at Brownsville and Texas Southmost College, Brownsville, TX 78520, USA
³⁰Trinity University, San Antonio, TX 78212, USA
³¹Universität Hannover, D-30167 Hannover, Germany
³²Universitat de les Illes Balears, E-07122 Palma de Mallorca, Spain
³³University of Birmingham, Birmingham, B15 2TT, United Kingdom
³⁴University of Florida, Gainesville, FL 32611, USA
³⁵University of Glasgow, Glasgow, G12 8QQ, United Kingdom
³⁶University of Michigan, Ann Arbor, MI 48109, USA
³⁷University of Oregon, Eugene, OR 97403, USA
³⁸University of Rochester, Rochester, NY 14627, USA
³⁹University of Wisconsin-Milwaukee, Milwaukee, WI 53201, USA
⁴⁰Washington State University, Pullman, WA 99164, USA
⁴¹University of Manchester, Jodrell Bank Observatory, Macclesfield, Cheshire, SK11 9DL, United Kingdom
- (Dated: October 25, 2018)

We place direct upper limits on the amplitude of gravitational waves from 28 isolated radio pulsars by a coherent multi-detector analysis of the data collected during the second science run of the LIGO interferometric detectors. These are the first *direct* upper limits for 26 of the 28 pulsars. We use coordinated radio observations for the first time to build radio-guided phase templates for the expected gravitational wave signals. The unprecedented sensitivity of the detectors allow us to set strain upper limits as low as a few times 10^{-24} . These strain limits translate into limits on the equatorial ellipticities of the pulsars, which are smaller than 10^{-5} for the four closest pulsars.

PACS numbers: 04.80.Nn, 95.55.Ym, 97.60.Gb, 07.05.Kf

^aCurrently at Stanford Linear Accelerator Center

^bCurrently at Jet Propulsion Laboratory

^cPermanent Address: HP Laboratories

^dCurrently at Rutherford Appleton Laboratory

^eCurrently at University of California, Los Angeles

^fCurrently at Hofstra University

^gPermanent Address: GReCO, Institut d'Astrophysique de Paris (CNRS)

A worldwide effort is underway to detect gravitational waves (GWs) and thus test a fundamental prediction of General Relativity. In preparation for long-term operations, the LIGO and GEO experiments conducted their first science run (S1) during 17 days in 2002. The detectors and the analyses of the S1 data are described in Refs. [1] and [2]-[5], respectively. LIGO's second science run (S2) was carried out from 14 Feb to 14 April 2003, with dramatically improved sensitivity compared to S1. During S2 the GEO detector was not operating.

A spinning neutron star is expected to emit GWs if it is not perfectly symmetric about its rotation axis. The strain amplitude h_0 of the emitted signal is proportional to the star's deformation as measured by its ellipticity ϵ [6]. Using data from S2, this paper reports *direct* observational limits on the GW emission and corresponding ellipticities from the 28 most rapidly rotating isolated pulsars for which radio data is complete enough to guide the phase of our filters with sufficient precision. These are the first such limits for 26 of the pulsars. We concentrate on isolated pulsars with known phase evolutions and sky positions to ensure that our targeted search requires relatively few unknown parameters.

The limits reported here are still well above the indirect limits inferred from observed pulsar spindown, where available (Fig. 1). However, fourteen of our pulsars are in globular clusters, where local gravitational accelerations produce Doppler effects that mask the intrinsic pulsar spindown, sometimes even producing apparent spinup. For these pulsars our observations therefore place the first limits that are inherently independent of cluster dynam-

ics, albeit at levels well above what one would expect if all globular cluster pulsars are similar to field pulsars.

Our most stringent ellipticity upper limit is 4.5×10^{-6} . While still above the maximum expected from conventional models of nuclear matter, distortions of this size would be permitted within at least one exotic theory of neutron star structure [7].

Detectors.—LIGO comprises three detectors. Each detector is a power-recycled Michelson interferometer, with Fabry-Perot cavities in the long arms. A passing GW produces a time-varying differential strain in these arms, and the resulting differential displacement of the cavity test mass mirrors is sensed interferometrically. Two detectors, the 4 km-arm H1 and the 2 km-arm H2 detectors, are collocated in Hanford WA. The 4 km-arm L1 detector is situated in Livingston Parish LA. Improvements in noise performance between S1 and S2 were approximately an order of magnitude over a broad frequency range. Modifications that were made between S1 and S2 to aid in noise reduction and improve stability include: i) increased laser power to reduce high-frequency noise, ii) better angular control of the mirrors of the interferometer and iii) the use of lower noise digital test mass suspension controllers in all detectors.

During S2, the LIGO detectors' noise performance in the band 40-2000 Hz was better than any previous interferometer. The best strain sensitivity, achieved by L1, was $\sim 3 \times 10^{-22} \text{ Hz}^{-1/2}$ near 200 Hz (where it translates through Eq. (2.2) of [2] into a detectable amplitude for a continuous signal of about 3×10^{-24} , as shown in Fig. 1). The relative timing stability between the interferometers was also significantly improved. Monitored with GPS-synchronized clocks to be better than $10 \mu\text{s}$ over S2, it allowed the coherent combination of the strain data of all three detectors to form joint upper limits.

Analysis method.—In [2] a search for gravitational waves from the millisecond pulsar J1939+2134 using S1 data was presented. In that work, two different data analysis methods were used, one in the time domain and the other in the frequency domain. Here we extend the former method [2, 8] and apply it to 28 isolated pulsars.

Following [2] we model the sources as non-precussing triaxial neutron stars showing the same rotational phase evolution as is present in the radio signal and perform a complex heterodyne of the strain data from each detector at the instantaneous frequency of the expected gravitational wave signal, which is twice the observed radio rotation frequency. These data are then down-sampled to 1/60 Hz and will be referred to as B_k . Any gravitational signal in the data would show a residual time evolution reflecting the antenna pattern of the detector, varying over the day as the source moved through the pattern, but with a functional form that depended on several other source-observer parameters: the antenna responses to plus and cross polarisations, the amplitude of the gravitational wave h_0 , the angle between the line-of-sight to the pulsar and its spin axis ι , the polarisation angle of the gravitational radiation ψ (all defined in [6]) and the phase ϕ_0 of the gravitational wave signal at some fiducial time t_0 . Let \mathbf{a} be a vector in parameter space

^hCurrently at Keck Graduate Institute

ⁱCurrently at National Science Foundation

^jCurrently at University of Sheffield

^kCurrently at Ball Aerospace Corporation

^lCurrently at European Gravitational Observatory

^mCurrently at Intel Corp.

ⁿCurrently at University of Tours, France

^oCurrently at Lightconnect Inc.

^pCurrently at W.M. Keck Observatory

^qCurrently at ESA Science and Technology Center

^rCurrently at Raytheon Corporation

^sCurrently at New Mexico Institute of Mining and Technology / Magdalena Ridge Observatory Interferometer

^tCurrently at Mission Research Corporation

^uCurrently at Harvard University

^vCurrently at Lockheed-Martin Corporation

^wPermanent Address: University of Tokyo, Institute for Cosmic Ray Research

^xPermanent Address: University College Dublin

^yCurrently at Research Electro-Optics Inc.

^zCurrently at Institute of Advanced Physics, Baton Rouge, LA

^{aa}Currently at Thirty Meter Telescope Project at Caltech

^{bb}Currently at European Commission, DG Research, Brussels, Belgium

^{cc}Currently at University of Chicago

^{dd}Currently at LightBit Corporation

^{ee}Permanent Address: IBM Canada Ltd.

^{ff}Currently at University of Delaware

^{gg}Permanent Address: Jet Propulsion Laboratory

^{hh}Currently at Shanghai Astronomical Observatory

ⁱⁱCurrently at Laser Zentrum Hannover

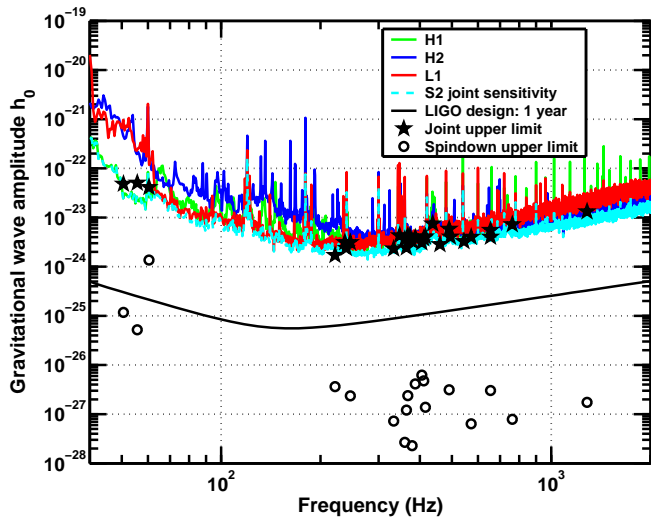


FIG. 1: Upper curves: h_0 amplitudes detectable from a known generic source with a 1% false alarm rate and 10% false dismissal rate, as given by Eq. (2.2) in [2] for single detector analyses and for a joint detector analysis. All the curves use typical S2 sensitivities and observation times. H1 and H2 are the 4 km-arm and the 2 km-arm detectors located in Hanford WA. L1 is the 4 km-arm detector situated in Livingston Parish LA. Lower curve: LIGO design sensitivity for 1 yr of data. Stars: upper limits found in this paper for 28 known pulsars. Circles: spindown upper limits for the pulsars with negative frequency derivative values if *all* the measured rotational energy loss were due to gravitational waves and assuming a moment of inertia of 10^{45} g cm^2 .

with components $(h_0, \iota, \psi, \phi_0)$.

The analysis proceeds by determining the posterior probability distribution function (pdf) of \mathbf{a} given the data B_k and the signal model:

$$p(\mathbf{a}|\{B_k\}) \propto p(\mathbf{a})p(\{B_k\}|\mathbf{a}), \quad (1)$$

where $p(\{B_k\}|\mathbf{a})$ is the likelihood and $p(\mathbf{a})$ the prior pdf we assign to the model parameters. We have used a uniform prior for $\cos \iota$, ϕ_0 , ψ and h_0 ($h_0 > 0$), in common with [2]. A uniform prior for h_0 has been chosen for its simplicity and so that our results can readily be compared with other observations. This prior favors high values of h_0 (which comprise the majority of the parameter space) and therefore generates a somewhat conservative upper limit for its value. Indeed the reader might prefer to regard our resulting posterior pdfs for h_0 as marginalised likelihoods rather than probabilities for h_0 — these are functionally identical using our priors.

As in [2] we use a Gaussian joint likelihood for $p(\{B_k\}|\mathbf{a})$. In [2] the S1 noise floor was estimated over a 60 s period from a 4 Hz band about the expected signal frequency. This gave a reliable point estimate for the noise level but was sensitive to spectral contamination within the band, as demonstrated in the analysis of the GEO S1 data. In this paper we exploit the improved stationarity of the instruments that make it reasonable to assume the noise floor is constant over periods of 30 min [8]. In addition we restrict the bandwidth to 1/60 Hz,

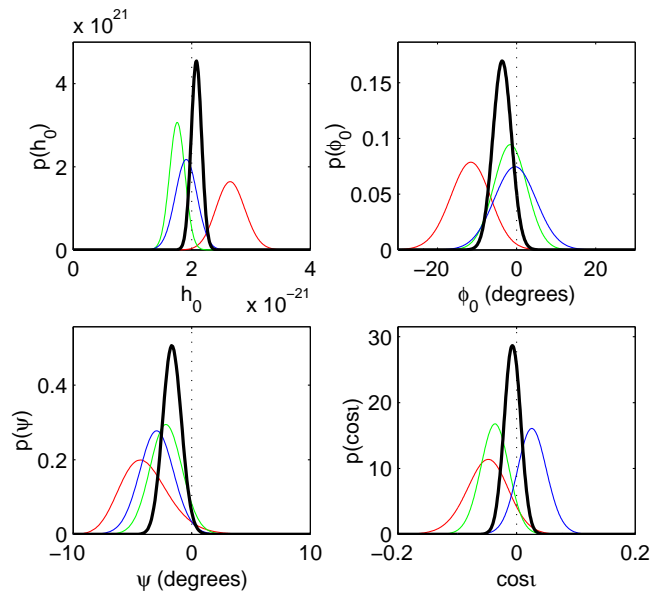


FIG. 2: Parameters of the artificial pulsar P1, recovered from 12h of strain data from the Hanford and Livingston interferometers. The results are displayed as marginal pdfs for each of the four signal parameters. The vertical dotted lines show the values used to generate the signal, the colored lines show the results from the individual detectors (H1 green, H2 blue, L1 red), and the black lines show the joint result from combining coherently data from all three.

which makes it possible to search for signals from pulsars at frequencies close to strong spectral disturbances. However, the noise level now determined is less certain as the estimate relies on fewer data. We take account of this increased uncertainty by explicitly marginalising with a Jeffreys prior over the constant but unknown noise level for each 30 min period of data [9]. The likelihood for this analysis is then the combined likelihood for all the 30 min stretches of data, labeled by j in Eq. (2), taken as independent:

$$p(\{B_k\}|\mathbf{a}) \propto \prod_j p(\{B_k\}_j|\mathbf{a}), \quad (2)$$

$$p(\{B_k\}_j|\mathbf{a}) \propto \left(\sum_{k=k_1(j)}^{k_2(j)} |B_k - y_k|^2 \right)^{-m}, \quad (3)$$

where y_k is the signal model given by Eq. (4.10) in [2] and $m = k_2(j) - k_1(j) + 1 = 30$ is the number of B_k data points in a 30 min segment.

In principle the period over which the data are assumed stationary need not be fixed, and can be adjusted dynamically to reflect instrumental performance over the run. We have limited our analysis to continuous 30 min stretches of data, which included more than 88% of the S2 science data set. Inclusion of shorter data sections would at best have resulted in a $\sim 6\%$ improvement on the strain upper limits reported here.

Validation by hardware injections.—All the software used in this analysis is available in the

LAL and LALapps CVS repositories (www.lsc-group.phys.uwm.edu/daswg/projects/lal.html) with the tag “pulgroup_paper_s2tds”. It was validated by checking its performance on fake pulsar signals injected in artificial and real detector noise, both in software ([2]) and in hardware. In particular, two artificial signals (P1, P2) were injected into all three detectors by modulating the mirror positions via the actuation control signals with the strain signal we should expect from a hypothetical pulsar. These injections were designed to give an end-to-end validation of the search pipeline starting from as far up the observing chain as possible.

The pulsar signals were injected for 12h at frequencies of 1279.123 Hz (P1) and 1288.901 Hz (P2) with frequency derivatives of zero and -10^{-8} Hz s $^{-1}$ respectively, and strain amplitudes of 2×10^{-21} . This gives signal-to-noise ratios (as defined by Eq. (79) of [6]) of 26 and 40 for P1 in H1 and L1 respectively and of 38 and 34 for P2. The signals were modulated and Doppler shifted to simulate sources at fixed positions on the sky with $\psi = 0$, $\cos \iota = 0$ and $\phi_0 = 0$. To illustrate, posterior pdfs for the recovered P1 signal are shown in Fig. 2. The results derived from the different detectors are in broad statistical agreement, confirming that the relative calibrations are consistent and that the assessments of uncertainty (expressed in the posterior widths) are reasonable. Results for P2 were very similar to these.

The phase stability of the detectors in S2 allowed us to implement a *joint* coherent analysis based on data from all three participating instruments. This technique was noted in [2], but could not be performed on the S1 data because of timing uncertainties that existed when those observations were performed. The black lines in Fig. 2 show marginalisations of the joint posterior from H1, H2 and L1, i.e.,

$$p(\mathbf{a}|\text{H1, H2, L1}) \propto p(\mathbf{a})p(\text{H1}|\mathbf{a})p(\text{H2}|\mathbf{a})p(\text{L1}|\mathbf{a}). \quad (4)$$

In an ideal case of three detectors of similar sensitivities and operational times these coherent results would be approximately $\sqrt{3}$ times tighter than the individual results. The posteriors for ϕ_0 clearly highlight the relative coherence between the instruments and verify that similar joint methods can be used to set upper limits on our target pulsars.

Results.—From the ATNF pulsar catalogue (www.atnf.csiro.au/research/pulsar/psrcat/) we selected 28 isolated pulsars with rotational frequencies greater than 20 Hz and for which sufficiently good timing data were available (Table I). For 18 of these, we obtained updated timing solutions from regular timing observations made at the Jodrell Bank Observatory using the Lovell and the Parkes telescopes, adjusted for a reference epoch centred on the epoch of the S2 run (starred pulsars in Table I). Details of the techniques that were used to do this can be found in [10]. We also checked that none of these pulsars exhibited a glitch during this period.

The list includes globular cluster pulsars (including isolated pulsars in 47 Tuc and NGC6752), the S1 target millisecond pulsar (J1939+2134) and the Crab pul-

pulsar	spin f (Hz)	spindown \dot{f} (Hz s $^{-1}$)	$h_0^{95\%}$ / 10^{-24}	ϵ / 10^{-5}
B0021–72C*	173.71	$+1.50 \times 10^{-15}$	4.3	16
B0021–72D*	186.65	$+1.19 \times 10^{-16}$	4.1	14
B0021–72F*	381.16	-9.37×10^{-15}	7.2	5.7
B0021–72G*	247.50	$+2.58 \times 10^{-15}$	4.1	7.5
B0021–72L*	230.09	$+6.46 \times 10^{-15}$	2.9	6.1
B0021–72M*	271.99	$+2.84 \times 10^{-15}$	3.3	5.0
B0021–72N*	327.44	$+2.34 \times 10^{-15}$	4.0	4.3
J0030+0451	205.53	-4.20×10^{-16}	3.8	0.48
B0531+21*	29.81	-3.74×10^{-10}	41	2100
J0711–6830	182.12	-4.94×10^{-16}	2.4	1.8
J1024–0719*	193.72	-6.95×10^{-16}	3.9	0.86
B1516+02A	180.06	-1.34×10^{-15}	3.6	21
J1629–6902	166.65	-2.78×10^{-16}	2.3	2.7
J1721–2457	285.99	-4.80×10^{-16}	4.0	1.8
J1730–2304*	123.11	-3.06×10^{-16}	3.1	2.5
J1744–1134*	245.43	-5.40×10^{-16}	5.9	0.83
J1748–2446C	118.54	$+8.52 \times 10^{-15}$	3.1	24
B1820–30A*	183.82	-1.14×10^{-13}	4.2	24
B1821–24*	327.41	-1.74×10^{-13}	5.6	7.1
J1910–5959B	119.65	$+1.14 \times 10^{-14}$	2.4	8.5
J1910–5959C	189.49	-7.90×10^{-17}	3.3	4.7
J1910–5959D	110.68	-1.18×10^{-14}	1.7	7.2
J1910–5959E	218.73	$+2.09 \times 10^{-14}$	7.5	7.9
J1913+1011*	27.85	-2.61×10^{-12}	51	6900
J1939+2134*	641.93	-4.33×10^{-14}	13	2.7
B1951+32*	25.30	-3.74×10^{-12}	48	4400
J2124–3358*	202.79	-8.45×10^{-16}	3.1	0.45
J2322+2057*	207.97	-4.20×10^{-16}	4.1	1.8

TABLE I: The 28 pulsars targeted in the S2 run, with approximate spin parameters. Pulsars for which radio timing data were taken over the S2 period are starred (*). The right-hand two columns show the 95% upper limit on h_0 , based on a coherent analysis using all the S2 data, and corresponding ellipticity values (ϵ , see text). These upper limit values do *not* include the uncertainties due to calibration and to pulsar timing accuracy, which are discussed in the text, nor uncertainties in the pulsar’s distance, r .

sar (B0531+21). Although Table I only shows approximate pulsar frequencies and frequency derivatives, further phase corrections were made for pulsars with measured second derivatives of frequency. Timing solutions for the Crab were taken from the Jodrell Bank online ephemeris [11], and adjustments were made to its phase over the period of S2 using the method of [12].

The analysis used 910 hours of data from H1, 691 hours from H2, and 342 hours from L1. There was no evidence of strong spectral contamination in any of the bands investigated, such as might be caused by an instrumental feature or a potentially detectable pulsar signal. A strong gravitational signal would generate a parameter pdf prominently peaked off zero with respect to its width, as for the hardware injections. Such a pdf would trigger

a more detailed investigation of the pulsar in question. No such triggers occurred in the analysis of these data, and we therefore present upper limits.

The upper limits are presented as the value of h_0 bounding 95% of the cumulative probability of the marginalised strain pdf from $h_0 = 0$. The joint upper limit $h_0^{95\%}$ therefore satisfies

$$0.95 = \int_{h_0=0}^{h_0^{95\%}} dh_0 \iiint p(\mathbf{a}|\text{H1, H2, L1}) d\iota d\psi d\phi_0, \quad (5)$$

consistent with [2]. The uncertainty in the noise floor estimate is already included, as outlined above.

The remaining uncertainties in the upper limit values of Table I stem from the calibration of the instrument and from the accuracy of the pulsar timing models. For L1 and H2, the amplitude calibration uncertainties are conservatively estimated to be 10% and 8%, respectively. For H1, the maximum calibration uncertainty is 18%, with typical values at the 6% level. Phase calibration uncertainties are negligible in comparison: less than 10° in all detectors. Biases due to pulsar timing errors are estimated to be 3% or less for J0030+0451, and 1% or less for the remaining pulsars (see [2] for a discussion of the effect of these uncertainties).

Discussion.—The improved sensitivity of the LIGO interferometers is clear from the strain upper limit for PSR J1939+2134, which is more than a factor of ten lower than was achieved with the S1 data [2]. In this analysis the lowest limit is achieved for PSR J1910–5959D at the level of 1.7×10^{-24} , largely reflecting the lower noise floor around 200 Hz.

Table I also gives approximate limits to the ellipticities [6] of these pulsars from the simple quadrupole model

$$\epsilon \simeq 0.237 \frac{h_0}{10^{-24}} \frac{r}{1 \text{ kpc}} \frac{1 \text{ Hz}^2}{f^2} \frac{10^{45} \text{ g cm}^2}{I_{zz}} \quad (6)$$

where r is the pulsar’s distance, which we take as the dispersion measure distance using the model of Taylor

and Cordes [13], and I_{zz} its principal moment of inertia about the rotation axis, which we take as 10^{45} g cm^2 .

As expected, none of these upper limits improves on those inferred from simple arguments based on the gravitational luminosities achievable from the observed loss of pulsar rotational kinetic energy. However, as discussed in the introduction, for pulsars in globular clusters such arguments are complicated by cluster dynamics, which the direct limits presented here avoid.

The result for the Crab pulsar (B0531+21) is within a factor of about 30 of the spindown limit and over an order of magnitude better than the previous direct upper limit of [14]. The equatorial ellipticities of the four closest pulsars (J0030+0451, J2124+3358, J1024–0719, and J1744–1134) are constrained to be less than 10^{-5} .

Once the detectors operate at design sensitivity for a year, the observational upper limits will improve by more than an order of magnitude. The present analysis will also be extended to include pulsars in binary systems, significantly increasing the population of objects under inspection.

Acknowledgments.—The authors gratefully acknowledge the support of the United States National Science Foundation for the construction and operation of the LIGO Laboratory and the Particle Physics and Astronomy Research Council of the United Kingdom, the Max-Planck-Society and the State of Niedersachsen/Germany for support of the construction and operation of the GEO600 detector. The authors also gratefully acknowledge the support of the research by these agencies and by the Australian Research Council, the Natural Sciences and Engineering Research Council of Canada, the Council of Scientific and Industrial Research of India, the Department of Science and Technology of India, the Spanish Ministerio de Ciencia y Tecnologia, the John Simon Guggenheim Foundation, the Leverhulme Trust, the David and Lucile Packard Foundation, the Research Corporation, and the Alfred P. Sloan Foundation. This document has been assigned LIGO Laboratory document number LIGO-P040008-B-Z.

-
- [1] B. Abbott et al. (The LIGO Scientific Collaboration), Nuclear Inst. and Methods in Physics Research A **517/1-3** 154 (2004).
 - [2] B. Abbott et al. (The LIGO Scientific Collaboration), Phys. Rev. D **69** 082004 (2004).
 - [3] B. Abbott et al. (The LIGO Scientific Collaboration), Phys. Rev. D **69** 122001 (2004).
 - [4] B. Abbott et al. (The LIGO Scientific Collaboration), Phys. Rev. D **69** 102001 (2004).
 - [5] B. Abbott et al. (The LIGO Scientific Collaboration), Phys. Rev. D **69** 122004 (2004).
 - [6] P. Jaranowski, A. Królak and B. Schutz, Phys. Rev. D **58** 063001 (1998).
 - [7] B.J. Owen, submitted to Phys. Rev. Lett.
 - [8] R. Dupuis, PhD thesis, University of Glasgow (2004).
 - [9] G.L. Bretthorst “Bayesian spectrum analysis and parameter estimation” Lecture Notes in Statistics, Vol 48 (Springer-Verlag, Berlin) (1988).
 - [10] G. Hobbs, A.G. Lyne, M. Kramer, C.E. Martin, and C. Jordan, Mon. Not. R. Astron. Soc. **353** 1311 (2004).
 - [11] Jodrell Bank Crab Pulsar Timing: Monthly Ephemeris, <http://www.jb.man.ac.uk/research/pulsar/crab.html>.
 - [12] M. Pitkin and G. Woan, Classical and Quantum Gravity **21** S843 (2004).
 - [13] J.H. Taylor and J.M. Cordes, ApJ **411** 674 (1993).
 - [14] T. Suzuki, in *First Edoardo Amaldi Conference on Gravitational Wave Experiments*, edited by E. Coccia, G. Pizzella and F. Ronga (World Scientific, Singapore, 1995), p. 115.